

## Cation ordering induced polarization enhancement for PbTiO<sub>3</sub>-SrTiO<sub>3</sub> ferroelectric-dielectric superlattices

Junkai Deng,<sup>1</sup> Alex Zunger,<sup>2</sup> and Jefferson Zhe Liu<sup>3,\*</sup>

<sup>1</sup>State Key Laboratory for Mechanical Behavior of Materials, Xi'an Jiaotong University, Xi'an 710049, China

<sup>2</sup>University of Colorado, Boulder, Colorado 80309, USA

<sup>3</sup>Department of Mechanical and Aerospace Engineering, Monash University, Clayton, Victoria 3800, Australia

(Received 3 December 2013; revised manuscript received 19 January 2015; published 17 February 2015)

In this Rapid Communication, an efficient computational material design approach (cluster expansion) is employed for the ferroelectric PbTiO<sub>3</sub>/SrTiO<sub>3</sub> system. Via exploring a configuration space including over  $3 \times 10^6$  candidates, two special cation ordered configurations—either perfect or mixed 1/1 (011) superlattice—are identified with the mostly enhanced ferroelectric polarization by up to about 95% in comparison with the (001) superlattice. We find that the exotic couplings between the antiferrodistortive (AFD) and ferroelectric (FE) modes (e.g., AFD<sub>x</sub>-FE<sub>z</sub> and AFD<sub>xy</sub>-FE<sub>z</sub>), which is absent from the PTO and STO, as the origin for the best polarization property of the two superlattices. This understanding should provide fresh ideas to design multifunctional perovskite heterostructures.

DOI: [10.1103/PhysRevB.91.081301](https://doi.org/10.1103/PhysRevB.91.081301)

PACS number(s): 77.55.Px, 61.66.Dk, 77.22.Ej

*Searching a large space of superlattice configurations for the one having target properties.* Advances in layer-by-layer growth from oxide building blocks  $(X)_n/(Y)_m$  [1,2] now permit laboratory realization of numerous layer sequences  $(n, m, n', m' \dots)$ , each having, in principle, different, configuration-dependent physical properties not normally accessible by the isolated end-point components. However, since the number of possible configurations  $\sigma$  ( $\sim 2^N$ , possible from a  $N$  unit-cell two-component superlattice) far exceeds what could be practically grown exhaustively, the search for the “magic configuration”  $\sigma^*$  having desired target properties has generally been reduced to sporadic explorations of just a tiny fraction of this astronomic space, often inspecting just a few simple periods  $(n, m)$  such as (1,1), (2,2), and (2,3) [3]. Here we focus on the computational search of  $\sim 3 \times 10^6$  heterostructure configurations realizable from the  $X = \text{PbTiO}_3$  and  $Y = \text{SrTiO}_3$  building blocks that has the maximal ferroelectric polarization  $P$  possible in this space. We do so by first calculating via density functional theory (DFT) the polarization  $P_{\text{DFT}}(\sigma)$  of  $\sim 50$  configurations and using this knowledge to construct a robust cluster expansion (CE)  $P_{\text{CE}}(\sigma)$  that captures with precision of 3% the polarization  $P_{\text{DFT}}(\sigma)$  of configurations included as well as excluded from the fit. Since evaluation of  $P_{\text{CE}}(\sigma)$  for a given  $\sigma$  takes  $10^{-5}$  of the typical effort needed to calculate  $P_{\text{DFT}}(\sigma)$ , this CE can now be searched almost effortlessly for  $\sim 3\,000\,000$  configurations ( $N < 20$ ), thus readily identifying the magic configurations  $\sigma^* = (\text{PbTiO}_3)_1/(\text{SrTiO}_3)_1$  and  $(\text{Pb}_{0.5}\text{Sr}_{0.5}\text{TiO}_3)_1/(\text{SrTiO}_3)_1$  both along the (011) direction as having a [001] polarization value  $\sim 55\%$  higher than the linear interpolation of the two end-point constituents, and  $\sim 40\%$  higher than the random alloy, and  $\sim 95\%$  higher than the (001) superlattices. This approach allows us to focus on the analysis of new physical mechanisms directly for the configurations that matter, not for arbitrary configurations that may or may not have new physics. We analyze the physical origins of what makes

these best candidates special, finding that the enhancement in ferroelectric polarization originates from a surprising effect previously overlooked in perovskite heterostructure, i.e., the antiferrodistortive-ferroelectric (AFD<sub>x</sub>-FE<sub>z</sub> or AFD<sub>xy</sub>-FE<sub>z</sub>) coupling, unique to the superlattice interfaces and absent from the building blocks PTO and STO. This understanding could allow, in the future, the introduction of exotic AFD-FE couplings via heterostructure design for novel multifunctional perovskite materials, e.g., multiferroics [1,4].

*DFT calculation of the polarization.* First-principles calculations based on DFT were performed using the local density approximation [5] and the projector augmented wave method [6] implemented in the Vienna *ab initio* simulation package [7]. The use of periodic boundary conditions imposed short-circuit electrical conditions. The in-plane lattice constant was fixed to 3.864 Å to account for the constraint from a cubic STO substrate. All ionic positions were relaxed until the forces were less than 5 meV/Å. Due to a small lattice mismatch of STO and PTO (<0.05%), the constraint effects on  $P$  and total energy are insignificant. The electric polarization was computed by using the bulk Born effective charges [8], i.e.,  $Z_{\text{Pb,Sr}}^* = 2.7$  and  $Z_{\text{Ti}}^* = 4.6$  and the cation off-center displacement of fully relaxed configuration in DFT calculations. The selected values of bulk Born effective charges yielded an excellent agreement with results using the Berry phase method [8].

*Constructing an expansion for polarization as a function of configuration.* The CE approach [9,10] can map the relations between different configurations and their physical properties. For a binary mixture, one defines a configuration  $\sigma$  as a specific decoration of two types of building units on a given Bravais lattice, in which each lattice site is occupied by either of the two (spin variable  $s_i = -1$  or  $= 1$ , respectively). The property of interest  $\mathcal{F}$  can then be expressed as

$$\mathcal{F}_{\text{CE}}(\sigma) = J_0 + \frac{1}{N} \left[ \sum_i J_i s_i + \sum_{i,j} J_{ij} s_i s_j + \sum_{i,j,k} J_{ijk} s_i s_j s_k + \dots \right], \quad (1)$$

\*zhe.liu@monash.edu

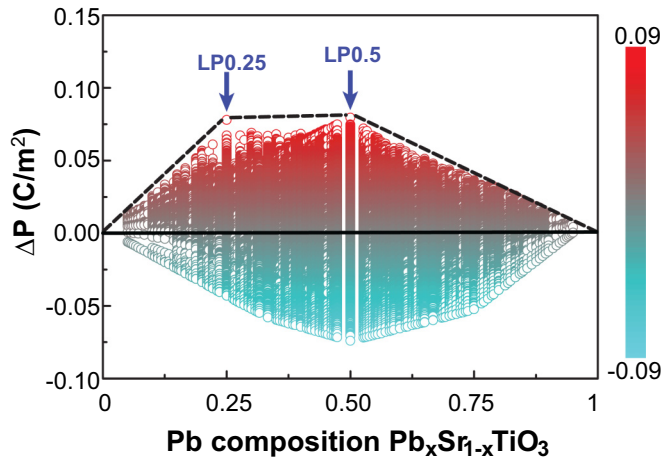


FIG. 1. (Color online) Polarization enhancement of PTO/STO configurations with respect to the concentration weighted average of bulk PTO and STO,  $\Delta P_{CE}(\sigma)$ , predicted by the cluster expansion approach. The two configurations at breaking points of the convex hull represent the optimal configurations with the largest polarization (LP) at PTO concentrations of 0.25 and 0.5 (named LP0.25 and LP0.5), respectively.

where  $J_{ij}, J_{ijk}, \dots$  represent the effective-cluster interactions (ECIs) for pair, three-body, ..., interactions in the chemical system, and the  $s_i s_j, s_i s_j s_k, \dots$  are the multisite cluster functions that form a complete basis set in the configuration space. The ECIs can be obtained by fitting the first-principles calculated results ( $\mathcal{F}$ ) of a set of ordered configurations to Eq. (1). The CE approach has been applied to total energy [9], Curie temperature [11], elastic modulus [12], thermoconductivity [13], and so on. It is applied here to ferroelectric polarization.

Using the data from DFT calculations, an iterative training process was used to fit the ECIs in Eq. (1) [14]. A good convergence was achieved with only 48 DFT inputs. The obtained  $P_{CE}(\sigma)$  includes 15 pairs, one triplet, three quadruplet, and one quintuplet clusters. The cross-validation score [15], representing the prediction error of  $P_{CE}(\sigma)$ , is less than  $0.011 \text{ C/m}^2$ .

Searching  $\sim 3\,000\,000$  configurations for identifying the one with the largest polarization. Figure 1 and Fig. S1 [16] show the polarization enhancement  $\Delta P_{CE}(\sigma)$  of the  $O(3 \times 10^6)$  ordered configurations with respect to the concentration weighted average of the bulk PTO and STO. The two breaking points of the convex hull (PTO concentrations of 0.25 and 0.5) represent the configurations of the largest polarization (LP) that exhibit the mostly enhanced  $P$  values. Their crystal structures are presented in Fig. 3 and Fig. S2 [16]. Their  $P$  values are 0.237 and  $0.392 \text{ C/m}^2$ , i.e., an enhancement of 95% and 71% in comparison with the counterpart (001) superlattices (SLs), respectively (Fig. S1) [16].

Careful inspection reveals a common cation ordering motif in Fig. 3 and Fig. S2 [16]. The LP0.5 is a perfect  $(\text{PbTiO}_3)_1/(\text{SrTiO}_3)_1$  (011) SL. The LP0.25 is an intermixed  $(\text{Pb}_{0.5}\text{Sr}_{0.5}\text{TiO}_3)_1/(\text{SrTiO}_3)_1$  (011) SL. Such special configurations were not expected before but successfully identified by CE. Note that the two LP configurations have a lower total energy than the (001) SL counterparts and other heterostructures

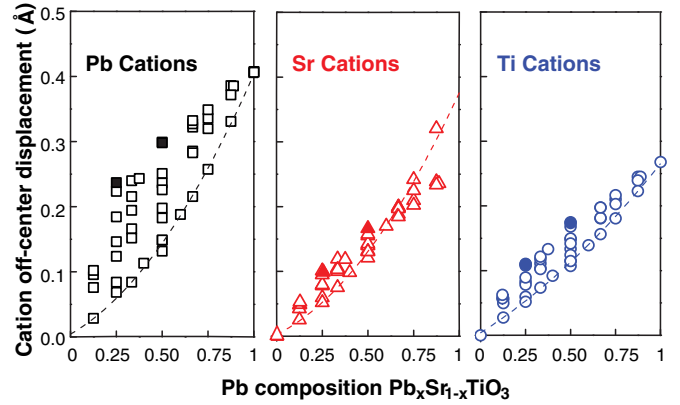


FIG. 2. (Color online) Average off-center displacements of (a) Pb, (b) Sr, and (c) Ti cations of the DFT calculated 48 configurations. The dashed lines are fitted to off-center displacements of the (001) superlattices.

(Table SIII) [16], suggesting that they should be feasible experimentally. In addition, experimental methods to grow short period (011) perovskite SLs were already demonstrated [17]. Since the short period structures explored here are expected to remain coherent, they would also be well within the currently available growth capabilities; their growth is thus called for.

*The mechanism leading to maximal polarization—AFD-FE coupling in the LP configurations.* The roles of different cations in determining the FE polarization can be seen in Fig. 2, where averaged cation off-center displacements of the 48 configurations calculated using DFT are summarized. The dashed lines in Fig. 2 depict results for the (001) PTO/STO superlattices. The solid symbols represent results for those two LP configurations (Fig. 1), indicating the largest cation off-center displacements (thus the largest FE polarization). A much less variation of the averaged Sr and Ti off-center displacements among configurations suggests the primary role of the Pb cations.

To elucidate the origin of the enhanced polarization of the LP configurations, the relaxed crystal structures of LP0.5 and LP0.25 (Fig. 3) are carefully examined using the symmetry mode analysis program ISOTROPY suite [18]. The results are summarized in Fig. 3, Table I, and Table SI [16]. Two primary AFD distortion modes of the LP0.5 are shown in Fig. 3(a). The  $\Gamma_4^+$  mode represents a tilting of octahedra about the  $x$  axis with a tilting angle of  $\theta = 2.9^\circ$ ; consequently in the (001) plane the oxygen atoms move away from the Pb and toward the Sr cations. The  $\Gamma_1^+$  mode represents a shape distortion of octahedra, i.e., the Ti-O bonds being bent toward the Sr cations in the  $yz$  plane. It is interesting to note that the two primary AFD modes of the LP0.25 [Fig. 3(b)],  $\Gamma_1^+$  and  $\Gamma_3^+$ , resemble those of LP0.5, except that in mode  $\Gamma_1^+$  the Ti-O bonds are bent in both the  $xz$  and  $yz$  planes and the octahedra tilting in  $\Gamma_3^+$  mode takes place along both the  $x$  and  $y$  axes.

To examine the coupling between the AFD and the FE modes, we artificially “turn off” these AFD modes in the LP structures meanwhile allowing the FE polarization to fully develop in DFT calculations. The results are shown in Table I. Turning off the minor distortion modes (“others”

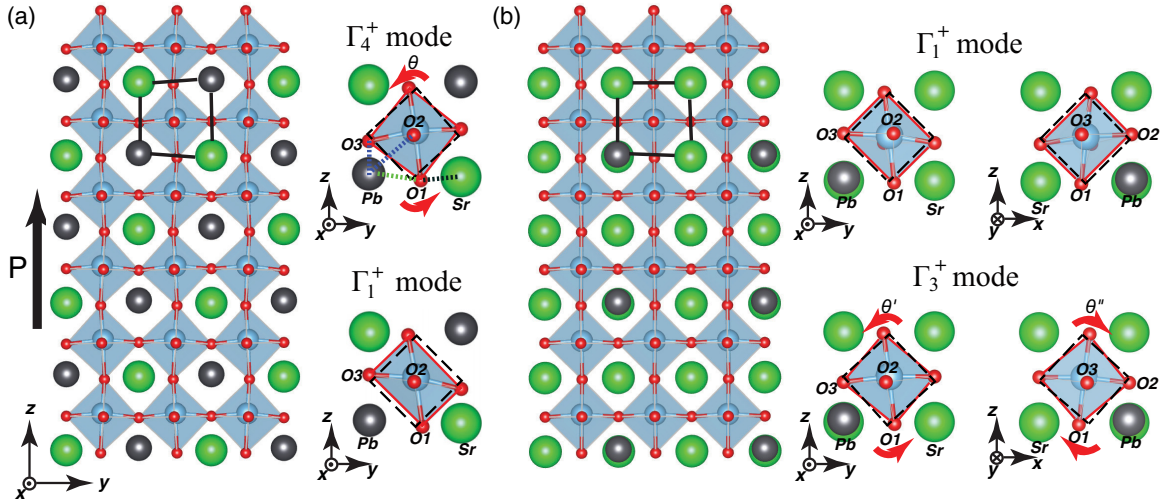


FIG. 3. (Color online) Relaxed structures and two primary AFD modes of the (a) LP0.5 and (b) LP0.25 in DFT calculations. In LP0.5, the primary mode  $\Gamma_4^+$  represents an octahedra tilting along the  $x$  axis with the oxygen atom in the (001) plane moving toward Sr cations (the Glazer notation  $a^+b^0b^0$ ). The secondary  $\Gamma_1^+$  mode represents a shape distortion of octahedra with oxygen atoms O1 and O3 moving toward Sr cations. Interestingly, the two primary modes of LP0.25,  $\Gamma_1^+$  and  $\Gamma_3^+$  (Glazer notation  $a^+a^+c^0$ ), resemble those of LP0.5 (see text for details).

in Table I and Table SI [16]) in LP0.5 slightly enhance the  $P$  to  $0.396 \text{ C/m}^2$ . It suggests that these AFD distortion modes indeed suppress the FE polarization, consistent with the traditional views in perovskites. In contrast,  $\Gamma_4^+$  and  $\Gamma_1^+$  modes promote the polarization, turning off of these two modes significantly reducing the polarization value down to  $0.354 \text{ C/m}^2$  together with an increase of total energy. The same conclusion can be drawn for LP0.25, i.e., the AFD modes enhancing the  $P$  values monotonously from  $0.209$  to  $0.237 \text{ C/m}^2$ . For the PTO/STO 1/1 or 2/2 (001) SLs, the out-of-plane AFD $_z$ -FE $_z$  coupling [4] and the in-plane AFD $_{xy}$ -FE $_{xy}$  coupling [19] have been observed. The discovered coupling between in-plane AFD $_x$  or AFD $_{xy}$  (i.e.,  $\Gamma_4^+$  in LP0.5 and  $\Gamma_3^+$  in LP0.25) and out-of-plane FE $_z$  modes in our LP structures has not been reported. Interestingly, these distortion modes and their couplings do not exist in the parent constituents, either. This observation gives us an important clue that *new distortion*

*modes and their couplings can be introduced via designing the heterostructures.*

Note that the LP configurations can be seen as intermixed (001) SLs (Fig. 3 and Fig. S2 [16]). It was proposed that by introducing some degree of interface cation mixing to a ferroelectric-dielectric superlattice could enhance FE polarization [8]. This is because to avoid the electrostatic energy penalty from the net charge accumulated at interfaces, the FE/dielectric layer will be depolarized/polarized to yield similar polarization values, often leading to a reduced total polarization value [4,8]. Introducing interlayer cation mixing could reduce the energy penalty and thus enhance the polarization  $P$ . In Table I, the intermixing effect of LP0.5 indeed reduces the total energy and increases the polarization significantly in comparison with the (001) SL, apparently supporting the model from Cooper *et al.* [8]. But an exception is observed for LP0.25. The intermixing does not reduce the total energy, whereas it significantly enhances the  $P$  value. Apparently there is no simple model to account for the interface mixing effect on FE polarization.

The AFD-FE coupling plays a decisive role in determining the LP structures. Our DFT calculations show that a Sr cation dopant in PbTiO $_3$  tends to attract oxygen atoms moving toward it (Fig. S4) [16,19]. For the LP0.5, the checkerboard cation ordering pattern in the  $yz$  plane [Fig. 3(a) and Fig. S2 [16]] ensures the two Sr cations (neighboring a Pb cation) can work collaboratively to maximize the  $\Gamma_4^+$  and  $\Gamma_1^+$  modes. In the LP0.25, the Pb cations show a BCC ordered pattern on the simple cubic Bravais lattice (Fig. S2 [16]), in which all six nearest neighbors of every Pb cation are the Sr cations. These Sr neighbors should work collaboratively to maximize the  $\Gamma_1^+$  and  $\Gamma_4^+$  modes. Structural analysis indicates that the LP0.5 and LP0.25 have the largest octahedra tilting angle and Ti-O-Ti bending angle among all the configurations studied in our DFT calculations at  $x = 0.25$  and  $0.50$  (Fig. S5 and Table SIII [16]), respectively. For a comparison, we noticed one specific structure str381 (Fig. S6 [16]), which has a very similar cation

TABLE I. FE polarization and relative total energy results of the LP0.5 and LP0.25 with the distortion modes subsequently turning off. A comparison is made with the perfect (001) SLs. In all the cases, the polarization is allowed to fully develop in DFT calculations.

	Modes	$P_z$ (C/m $^2$ )	$\Delta E_{rel}$ (meV/cell)
LP0.5	$\Gamma_4^+$ and $\Gamma_1^+$ and other	0.392	-15.36
	$\Gamma_4^+$ and $\Gamma_1^+$	0.396	-15.11
	$\Gamma_4^+$	0.381	-5.33
	Intermixing	0.354	-3.65
(001) 1/1 SL		0.229	0.0
LP0.25	$\Gamma_1^+$ and $\Gamma_3^+$ and other	0.237	-4.0
	$\Gamma_1^+$ and $\Gamma_3^+$	0.232	-3.95
	$\Gamma_1^+$	0.224	-3.54
	Intermixing	0.209	2.5
(001) 1/3 SL		0.122	0.0

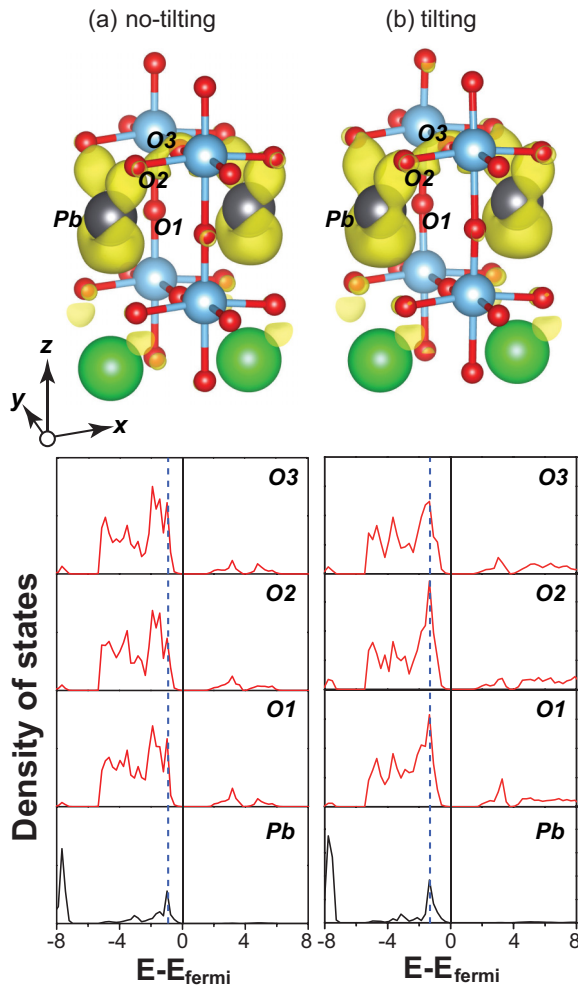


FIG. 4. (Color online) Difference-electron density and partial DOS for Pb and neighboring O ions in LP0.5 without octahedral tilts (a) and with tilting (b). The yellow isosurfaces are plotted at  $0.0045 e^-/\text{bohr}^3$ . In partial DOS results, black lines represent Pb 6s states and red lines represent O 2p states.

ordered pattern as LP0.5. If only considering the intermixing effect, the str381 has a lower total energy and a higher  $P$  value than those of LP0.5 (Table SIV [16]). But the small variation in ordered pattern results in a weaker collaborative effect, leading to a smaller tilting angle and Ti-O bending angle in str381 (Table SIII [16]). The AFD-FE coupling thus yields a larger  $P$  increase for the LP0.5 to overtake str381 as the LP configuration at  $x = 0.5$  (Table SIV [16]). We believe that the  $\text{AFD}_x\text{-FE}_z$  or  $\text{AFD}_{xy}\text{-FE}_z$  coupling is the origin for LP structures to have the largest polarization enhancement among the  $3 \times 10^6$  candidates. Interestingly, such unexpected coupling leads to the best FE polarization.

*Physical origins for the  $\text{AFD}_x\text{-FE}_z$  coupling.* Figure 4 shows the difference-electron density analysis and the projected partial density of states (pDOS) for Pb and its neighboring O ions in the LP0.5 (without/with  $\text{AFD}_x$ ). Clearly, the octahedra tilting can significantly enhance the hybridization between the Pb 6s and the O 2p orbitals, evidenced by the strongly overlapped peaks in pDOS and the strong charge redistribution among the Pb and O ions. For bulk PTO, it is well established that the hybridization between the Pb lone pair 6s electrons and the O 2p electrons induces its superior FE properties. The enhanced electronic hybridization caused by the  $\text{AFD}_x$  tilting is, therefore, the origin for the observed increase of  $\text{FE}_z$  polarization [19].

The importance of AFD-FE coupling has been recognized recently for designing multifunctional perovskite heterostructures, because the buckling of the interoctahedra B-O-B bond angles, a direct consequence of the octahedra rotation, can change physical properties, e.g., electronic bandwidth, magnetic interactions, and critical transition temperatures, etc. [20]. Some elegant design criteria have been proposed, but only considering a limited number of configurations such as the 1/1 and 2/2 (001) SLs, etc. [4,19,21–25]. In addition, those design rules adopt “interpolation” of the end-point components to study the SLs. In contrast, our studies show that heterostructures can have unique distortion modes and couplings that are absent from two end-point components, indicating unexplored rich and novel physics in perovskite systems. Our CE method can serve as a general and efficient means for discoveries and hence to help develop comprehensive design rules.

*Conclusions.* In summary, an efficient CE approach was used to study the cation ordering effects on the FE polarization in PTO/STO perovskite. Two (011) superlattices are identified as the configurations with the best polarization property. The exotic AFD-FE couplings (the in-plane  $\text{AFD}_x$  or  $\text{AFD}_{xy}$  modes and out-of-plane polarization  $\text{FE}_z$ ), unique to the SLs and not observed in either PTO or STO, are revealed as the origin for the best polarization  $P$ . This understanding provides fresh ideas in the design of other lone-pair driven ferroelectricity systems, exemplified by  $\text{BiFeO}_3$ , which is the most common mechanism to achieve the multiferroics in perovskite [1].

*Acknowledgments.* J.D. and J.Z.L. acknowledge the financial support from a Monash University Engineering faculty 2013 seed grant. J.D. also acknowledges the support of NSFC (Grants No. 51320105014 and No. 51471126), China Postdoctoral Science Foundation (Grant No. 2014M552435), and the Fundamental Research funds for the Central Universities. The work of A.Z. was funded by DOE, Office of Science, Basic Energy Science. The authors gratefully acknowledge computational support from Monash University Sun Grid and the National Computing Infrastructure funded by the Australian Government.

[1] R. Ramesh and N. A. Spaldin, *Nat Mater.* **6**, 21 (2007).  
 [2] J. C. Jiang, X. Q. Pan, W. Tian, C. D. Theis, and D. G. Schlom, *Appl. Phys. Lett.* **74**, 2851 (1999).

[3] M. Dawber, C. Lichtensteiger, M. Cantoni, M. Veithen, P. Ghosez, K. Johnston, K. M. Rabe, and J. M. Triscone, *Phys. Rev. Lett.* **95**, 177601 (2005).

- [4] E. Bousquet, M. Dawber, N. Stucki, C. Lichtensteiger, P. Hermet, S. Gariglio, J.-M. Triscone, and P. Ghosez, *Nature (London)* **452**, 732 (2008).
- [5] J. P. Perdew and A. Zunger, *Phys. Rev. B* **23**, 5048 (1981).
- [6] P. E. Blöchl, *Phys. Rev. B* **50**, 17953 (1994).
- [7] G. Kresse and J. Furthmüller, *Phys. Rev. B* **54**, 11169 (1996).
- [8] V. R. Cooper, K. Johnston, and K. M. Rabe, *Phys. Rev. B* **76**, 020103 (2007).
- [9] D. D. Fontaine, *Solid State Phys.* **47**, 33 (1994).
- [10] D. B. Laks, L. G. Ferreira, S. Froyen, and A. Zunger, *Phys. Rev. B* **46**, 12587 (1992).
- [11] A. Franceschetti, S. V. Dudiy, S. V. Barabash, A. Zunger, J. Xu, and M. van Schilfgaarde, *Phys. Rev. Lett.* **97**, 047202 (2006).
- [12] J. Z. Liu, A. van de Walle, G. Ghosh, and M. Asta, *Phys. Rev. B* **72**, 144109 (2005).
- [13] M. K. Y. Chan, J. Reed, D. Donadio, T. Mueller, Y. S. Meng, G. Galli, and G. Ceder, *Phys. Rev. B* **81**, 174303 (2010).
- [14] We started with feeding the  $P_{\text{DFT}}(\sigma)$  results of 23 usual suspects to fit the ECIs. Using the obtained  $P_{\text{CE}}(\sigma)$ , an exhaustive enumeration method was employed to search a configurational space [ $O(3 \times 10^6)$  configurations] for the LP configurations. The  $P_{\text{DFT}}$  results of these LP candidates, if not available, were then determined using DFT calculations and compared against the CE predictions. In the next iteration, these  $P_{\text{DFT}}$  results were added to the DFT data pool to refit the ECIs, and then the obtained  $P_{\text{CE}}(\sigma)$  was used to search for the new LP candidates. This iterative process was repeated until the CE predicted results agreed with the DFT calculations and no new LP configurations were predicted.
- [15] A. van de Walle and G. Ceder, *J. Phase Equilib.* **23**, 348 (2002).
- [16] See Supplemental Material at <http://link.aps.org/supplemental/10.1103/PhysRevB.91.081301> for total energy and FE polarization results of the PTO/STO heterostructures using DFT calculations, the AFD-FE coupling analysis, and some insights obtained from analyzing the LP configurations.
- [17] A. Annadi, Q. Zhang, X. Renshaw Wang, N. Tuzla, K. Gopinadhan, W. M. Lü, A. Roy Barman, Z. Q. Liu, A. Srivastava, S. Saha, Y. L. Zhao, S. W. Zeng, S. Dhar, E. Olsson, B. Gu, S. Yunoki, S. Maekawa, H. Hilgenkamp, T. Venkatesan, and Ariando, *Nat. Commun.* **4**, 1838 (2013).
- [18] B. J. Campbell, H. T. Stokes, D. E. Tanner, and D. M. Hatch, *J. Appl. Crystallogr.* **39**, 607 (2006).
- [19] P. Aguado-Puente, P. García-Fernández, and J. Junquera, *Phys. Rev. Lett.* **107**, 217601 (2011).
- [20] M. Imada, A. Fujimori, and Y. Tokura, *Rev. Mod. Phys.* **70**, 1039 (1998).
- [21] X. Wu, K. M. Rabe, and D. Vanderbilt, *Phys. Rev. B* **83**, 020104 (2011).
- [22] J. M. Rondinelli and C. J. Fennie, *Adv. Mater.* **24**, 1961 (2012).
- [23] J. M. Rondinelli, S. J. May, and J. W. Freeland, *MRS Bull.* **37**, 261 (2012).
- [24] J. M. Rondinelli and N. A. Spaldin, *Adv. Mater.* **23**, 3363 (2011).
- [25] A. T. Mulder, N. A. Benedek, J. M. Rondinelli, and C. J. Fennie, *Adv. Funct. Mater.* **23**, 4810 (2013).